Optics Letters

3-μm mid-infrared pulse generation using topological insulator as the saturable absorber

Jianfeng Li,[1,3,*] Hongyu Luo,[1] Lele Wang,[1] Chujun Zhao,[2] Han Zhang,[2] Heping Li,[1] and Yong Liu[1]

[1]State Key Laboratory of Electronic Thin Films and Integrated Devices, School of Optoelectronic Information, University of Electronic Science and Technology of China (UESTC), Chengdu 610054, China
[2]SZU-NUS Collaborative Innovation Center for Optoelectronic Science & Technology, Key Laboratory of Optoelectronic Devices and Systems of Ministry of Education and Guangdong Province, College of Optoelectronic Engineering, Shenzhen University, Shenzhen 518060, China
[3]Suzhou Institute of Biomedical Engineering and Technology, Chinese Academy of Sciences, Suzhou 215163, China
*Corresponding author: lijianfeng@uestc.edu.cn

Received 8 May 2015; revised 7 July 2015; accepted 17 July 2015; posted 20 July 2015 (Doc. ID 240558); published 31 July 2015

We report an 1150-nm diode-pump passively *Q*-switched Ho^{3+}-doped ZBLAN fiber laser using topological insulator (TI): Bi_2Te_3 as the saturable absorber (SA). The TI: Bi_2Te_3 prepared using the cost-effective hydrothermal intercalation/exfoliation method was dropped onto a CaF_2 substrate to fabricate the free-space SA component. It has a low saturable peak intensity of 2.12 MW/cm^2 and a high modulation depth of 51.3% measured at 2 μm. Inserting this component into a linear-cavity Ho^{3+}-doped ZBLAN fiber laser, stable *Q*-switched pulses at 2979.9 nm were obtained with the repetition rate of 81.96 kHz and pulse duration of 1.37 μs. The achieved maximum output power and pulse energy were 327.4 mW at a slope efficiency of 11.6% and 3.99 μJ, respectively, only limited by the available pump power. Our work reveals that the TIs are absolutely a class of promising and reliable SAs for pulse generation at 3-μm mid-infrared waveband.

OCIS codes: (140.3070) Infrared and far-infrared lasers; (140.3480) Lasers, diode-pumped; (140.3510) Lasers, fiber; (140.3540) Lasers, Q-switched; (160.4236) Nanomaterials.

http://dx.doi.org/10.1364/OL.40.003659

In recent years, mid-infrared fiber lasers at the waveband of 2–5 μm have attracted increasing attention owing to their potential applications in the areas of material processing [1], biomedical science [2], defense [3], nonlinear mid-infrared photonics [4], and inherent merits such as good beam quality, high-conversion efficiency, excellent heat dissipation, and compact packing. As a result, a series of research results toward improving laser power and energy [5,6], extending wavelength [7,8], and broadening spectrum [4] have been demonstrated. Compared to continuous-wave (CW) ones, pulsed fiber lasers can achieve high peak power and release large amounts of energy at short temporal range, thus enlarging their practical applications. Specifically, the emphasized ~3-μm pulsed fiber lasers have exhibited great potential in plastic, polymer processing, laser surgery, laser radar, etc. Concerning the methods of pulse generation, the passive scheme resorting to a SA is generally more favored owing to its compact and flexible structure in contrast to the active one, which usually requires an external driven modulator. To date, various material SAs have been fabricated and applied in the passive pulsed schemes at 3-μm waveband e.g., SESAM [9–12], Fe^{2+}:ZnSe crystal [13,14], and graphene [15]. Recently, we used a reversely designed InAs-based broadband SESAM to demonstrate a passively *Q*-switched 2.97-μm Ho^{3+}-doped and mode-locked 2.87-μm Ho^{3+}/Pr^{3+}-codoped ZBLAN fiber lasers for the first time [9,10]. Meanwhile, Wei *et al.* have demonstrated the *Q*-switched and mode-locked operations in fiber lasers at 3-μm waveband by utilizing the Fe^{2+}:ZnSe crystal and graphene as SAs [13–15].

Recently, a novel class of Dirac material known as TI arose and drew focused attention in the domain of condensed matters physics [16]. In the bulk state, TI has a nontrivial narrow-band gap while gapless metallic state in its edge/surface. In this contribution, its saturable absorption at a broadband range has also been demonstrated experimentally with the aid of the Pauli-blocking effect [17]. Since the first report on TI based pulse generation [18], a series of Tis, e.g., Bi_2Te_3, Bi_2Se_3, Sb_2Te_3, etc., have been widely employed in *Q*-switching and mode-locking of the fiber lasers at 1-μm, 1.5-μm and even 2-μm wavebands [19–22]. Therein, maximum output power of 22.35 mW [21] and maximum pulse energy of 1.525 μJ [22] have been obtained. Compared to SESAM and Fe^{2+}:ZnSe crystal, TI has a simple fabrication process and is easy to be integrated, especially it has a much broader absorption band. Compared to graphene, TI has a significantly higher modulation depth of typically as high as 98% (normalized) [18], and higher damage threshold [23], which are beneficial to achieve narrow and energetic *Q*-switched pulses. In this Letter, we report a high-energy passively *Q*-switched Ho^{3+}-doped ZBLAN fiber laser at 2979.9 nm using TI: Bi_2Te_3 as the SA for the first time to the best of pour knowledge.

In our experiment, TI: Bi_2Te_3 nanosheets were synthesized using the cost-effective hydrothermal intercalation/exfoliation method [24]. The ethanol solution dispersing the TI: Bi_2Te_3

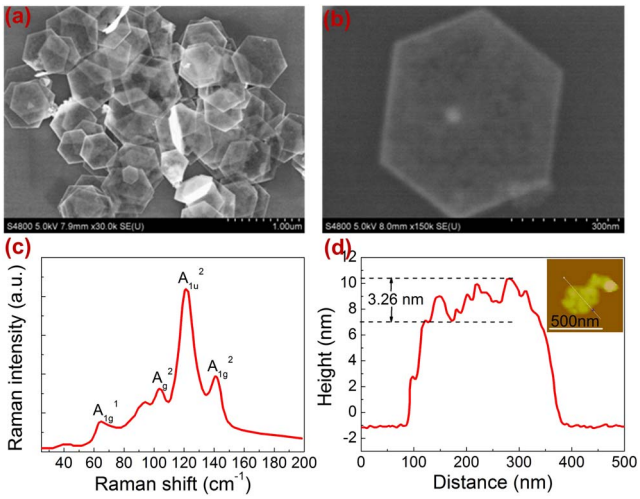

Fig. 1. (a) Lower and (b) higher magnification SEM images, (c) Raman spectrum, and (d) AFM image (inset) and its corresponding height profile of the TI: Bi_2Te_3 sample.

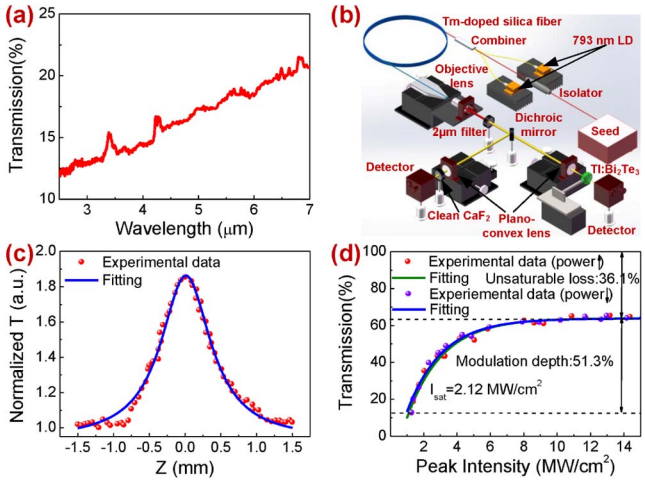

Fig. 2. (a) Infrared linear transmission spectrum, (b) experimental setup of TI: Bi_2Te_3 nonlinear transmission measurement at 2 μm, (c) Z-scan curve, and (d) nonlinear transmission as a function of incident peak intensity.

nanosheets were dropped on a CaF_2 substrate to fabricate the free-space SA component. Then a series of characterizations were performed to reveal the performance of our SA. Figures 1(a) and 1(b) show the measured SEM images of our TI: Bi_2Te_3 sample by field-emission scanning electron microscopy. The lower magnification SEM image as shown in Fig. 1(a) reveals many predominantly hexagonal-based sheets with uniform size and well-defined shape are randomly dispersed. The higher magnification SEM image as shown in Fig. 1(b) shows that the edge length of the sheets is at the range of 300–400 nm. Figure 1(c) is the measured Raman spectrum of our TI: Bi_2Te_3 sample. Three typical optical phonon peaks identified as A_{1g}^1, A_g^2, and A_{1g}^2 are located at 64.81 cm^{-1}, 103.43 cm^{-1}, 140.90 cm^{-1}, respectively. Besides, an additional peak A_{1u}^2 with strongest intensity locating at 121.20 cm^{-1} is also observed resulting from the symmetry breaking in atomically thin films. It indicates that the prepared TI: Bi_2Te_3 sample was in a great nano-structured state. Figure 1(d) shows the measured AFM image and its corresponding height profile of the TI: Bi_2Te_3 sample. The results suggest its average thickness is at the range of 7.11–10.37 nm.

Figure 2(a) shows the linear transmission spectrum of our TI: Bi_2Te_3 SA at the wavelength range of 2.5–7.0 μm measured using FT-IR spectrometer (Nicolet 6700) that has excluded the influence of CaF_2 substrate. It is observed that the transmission increases almost linearly from 11.8% to 20.8% with the wavelength except for some small fluctuations indicating its broadband potential. To investigate its nonlinear absorption, the Z-scan technology involving a balance twin-detector arrangement was employed to reduce the measurement errors, as shown in Fig. 2(b). Due to lack of a suitable 3-μm pulsed laser source with a high peak power, a homemade ultra-short pulsed laser source at 2 μm including a mode-locked Tm^{3+}-doped fiber laser seed and an amplifier was selected instead. It gave a repetition rate of 21.5 MHz, pulse duration of 1.51 ps, center wavelength of 1981.6 nm, FWHM of 2.76 nm, maximum average power of 84 mW, and signal-to-noise ratio (SNR) of >45 dB. The output beam from Tm^{3+}-doped silica fiber was collimated using a standard objective lens and then split into two orthogonal beams with 50:50 ratio by a 45° angle-placed dichroic mirror with respect to the incident beam after a 2-μm bandpass filter. Both beams were focused by two same plano-convex lenses with a focal length of 40 mm. For the left path, the power of the laser passing through a fixed clean CaF_2 substrate was monitored using one power meter to act as the reference. For the right path, the surface of the fabricated TI: Bi_2Te_3 SA was adjusted perpendicular to the focused beam axis. A linear motorized stage connected with a substrate mount was used to translate the SA along the beam axial direction and hence vary the spot size and peak intensity on the SA. The other power meter was placed after the SA to record the power. Upon dividing this power by the referenced power, a typical normalized Z-scan curve was achieved as shown in the Fig. 2(c). The sharp and narrow peak exhibits its excellent saturable absorption. Moreover, the nonlinear transmission of the SA as increased incident peak intensity was also measured at the position corresponding to the peak of the Z-scan curve where the beam spot diameter on the TI: Bi_2Te_3 SA was calculated to be ~60 μm, as shown in Fig. 2(d). In order to exclude the possibility of the TI: Bi_2Te_3 damage at high power state, its transmission was also measured with decreasing the incident peak intensity. The obtained reversible transmission variation indicated the TI: Bi_2Te_3 was free from damage. Thus, the relative parameters of our TI: Bi_2Te_3 SA can be obtained by fitting the measured data using the following formula:

$$T(I) = 1 - \Delta T \cdot \exp(-I/I_{sat}) - T_{ns}, \quad (1)$$

where $T(I)$ is the transmission, ΔT is the modulation depth, I is the incident peak intensity, I_{sat} is the saturable peak intensity, and T_{ns} is the nonsaturable loss. The calculated saturable peak intensity is 2.12 MW/cm^2, which is lower than 6.5 MW/cm^2 measured at 1550 nm [25]. This is because the TI is easier to be bleached at 2 μm as a result of the smaller band gap according to the band-filling principle. The calculated modulation depth of up to 51.3% might result from the combined contributions of the surface metallic and the insulating bulk states. It is larger than that measured at 1550 nm as a result of the differences in

material thickness [25]. The unsaturable loss is calculated to be 36.1%. Note that the nonlinear transmission curves excluded the influence of the CaF_2 substrate and were also not normalized. Thus, they can well reveal the dependence of the absolute transmission of our TI: Bi_2Te_3 SA on its corresponding incident peak intensity. Though the modulation depth of the TI: Bi_2Te_3 SA at 3 μm was not measured directly, a slightly lower value can be reasonably predicted according to its linear transmission.

The experimental setup of our constructed passively Q-switched Ho^{3+}-doped ZBLAN fiber laser based on TI: Bi_2Te_3 SA is shown in Fig. 3. Two commercially available high-power 1150-nm diode lasers (Eagleyard Photonics, Berlin) were employed to pump the gain fiber after polarization multiplexing via a polarized beam splitter (PBS) and focusing by a 1150-nm AR-coated ZnSe objective lens (Innovation Photonics, LFO-5-6-0.975/3 μm, 0.25 NA) with a 6.0-mm focal length acting as the collimator for the light out-coupled from the fiber core as well. A dichroic mirror (96%T at 1150 nm, 95%T at ~3 μm) was placed between the PBS and ZnSe objective lens at an angle of 45° with respect to the pump beam to direct the laser output. A 3-μm filter with a FWHM of 500 nm was used to block the residual pump. The gain fiber (Fiberlabs, Japan) was a piece of commercial double-cladding Ho^{3+}-doped ZBLAN fiber having a circular-shaped pump core with a diameter of 123 μm and NA of 0.5. The diameter and NA of the fiber core were 10 μm and 0.16, respectively. The dopant concentration was 2.0 mol. %, thus the selected 5.2-m fiber can provide 92% pump absorption efficiency. In this case, the fiber end close to the pump was perpendicularly cleaved acting as output coupler with the aid of 4% Fresnel reflection. The other fiber end was cleaved at an angle of 8° to avoid the parasitic lasing. The light from the angle-cleaved end was collimated via another specifically coating-designed ZnSe objective lens having a >95% transmission at 3 μm and <10% transmission at 1150 nm and finally terminated by a commercial broadband gold protected mirror. A confocal arrangement consisting of two same plano-covex CaF_2 lens with a focal length of 40 mm was inserted between the above ZnSe objective lens and protected gold mirror along the light path. The fabricated TI: Bi_2Te_3 SA component was first fixed in a mount connected with a one-dimension mobile platform along the light path and then placed in the confocal arrangement with an optimized position. An InAs detector with a response time of 2 ns driven by an in-house designed circuit was employed and connected with a 500-MHz bandwidth digital oscilloscope to record the pulse temporal waveform. A radio frequency (RF) spectrum analyzer (Advantest R3267) with a resolution bandwidth of 10 Hz to 100 MHz was used to measure the signal-to-noise ratio (SNR) of the pulses. A monochromator with a scanning resolution of 0.1 nm (Princeton instrument Acton SP2300) was utilized to measure the laser spectrum.

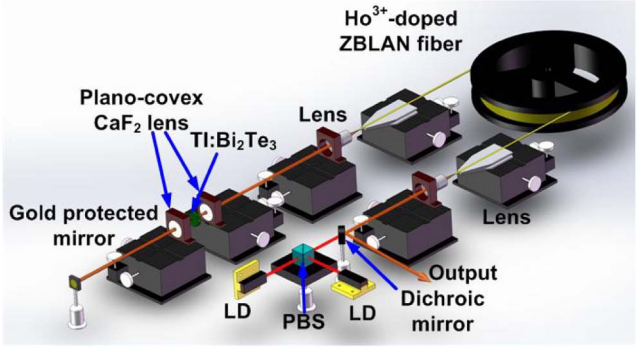

Fig. 3. Experimental setup of the passively Q-switched Ho^{3+}-doped ZBLAN fiber laser based on the TI: Bi_2Te_3 SA. LD is the 1150-nm laser diode, and PBS is the polarized beam splitter.

The CW laser was first produced when the launched pump power was increased to 270 mW. Once it reached 464 mW, stable Q-switching was observed with a pulse duration of 4.83 μs and a repetition rate of 46.20 kHz, as shown in Figs. 4(a) and 4(c). The stable Q-switching regime can be maintained until the maximum available launched pump power of 3.10 W, as shown in Figs. 4(b) and 4(c). The pulse duration and repetition rate were measured to be 1.37 μs and 81.96 kHz, respectively. The pulse amplitude fluctuation was calculated to be about ±3% indicating its high stability. The optical spectrum of the Q-switched pulses at the maximum pump power was measured and normalized, as shown in Fig. 4(d). The average wavelength of 2979.9 nm with a FWHM of 7.2 nm was obtained. The inset of Fig. 4(d) is the measured RF spectrum of the Q-switched pulses at a scanning span of 60 kHz and a resolution bandwidth of 100 Hz. The SNR of 37.4 dB indicates the stable Q-switching. At this moment, whether removing the TI: Bi_2Te_3 SA away from the cavity or moving the focused beam spot onto the clean region of the TI: Bi_2Te_3 partly covered CaF_2 substrate, the laser immediately recovered to the CW emission state identified by the oscilloscope due to lack of modulation factor. Note that the laser temporal performance in both cases was also monitored during the whole available pump range, and the unchanged CW emission state excluded the possibility of self-pulsing. The corresponding optical spectrum at the launched pump power of 3.10 W was also measured and shown in Fig. 4(d) as a comparison. The average wavelength was red-shifted to 2983.5 nm as a result of the decreased intra-cavity loss, which led to a lower initial Stark

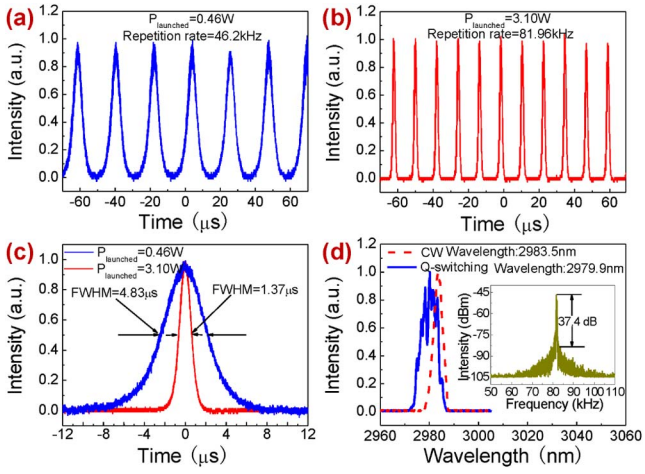

Fig. 4. Q-switched pulse train at the launched pump power of (a) 0.46 W and (b) 3.10 W, (c) Q-switched single-pulse waveform at the launched pump power of 0.46 W and 3.10 W, (d) optical spectra of CW laser and Q-switched pulses and RF spectrum (inset) of the Q-switched pulses at the launched pump power of 3.10 W.

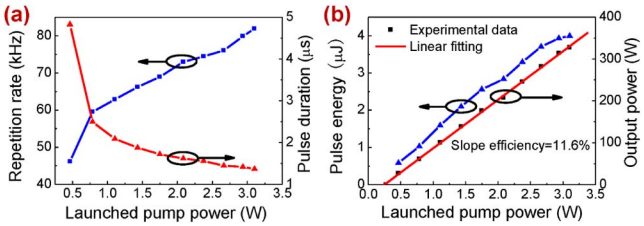

Fig. 5. (a) Repetition rate and pulse duration and (b) output power and single-pulse energy as a function of the launched pump power.

manifold of the $^5I_6$ energy level. Meanwhile, the spectrum bandwidth was narrowed to 4.4 nm owing to the less-required Fourier spectral components for CW emission.

Figure 5(a) shows the repetition rate and pulse duration of the *Q*-switched pulses as a function of the launched pump power. The repetition rate increases near linearly from 46.20 kHz to 81.96 kHz as increased launched pump power from 464 mW to 3.10 W owing to the faster population built-up on $^5I_6$ level. Meanwhile, the pulse duration decreases from 4.83 μs to 1.37 μs nonlinearly resulting from the more population-density accumulation on $^5I_6$ level. Both of them are the typical features of passive *Q*-switching. Figure 5(b) shows the measured output power and calculated single-pulse energy as a function of the launched pump power. It is observed that the output power and pulse energy increase near linearly with the launched pump power. The maximum output power of 327.38 mW at a slope efficiency of 11.6% and single-pulse energy of 3.99 μJ were achieved, only limited by the available pump power. Note that the TI: Bi_2Te_3 SA was not damaged even at such the high power level.

In conclusion, a passively *Q*-switched Ho^{3+}-doped ZBLAN fiber laser at 2979.9 nm employing TI: Bi_2Te_3 as the SA was demonstrated for the first time to the best of our knowledge. At the available maximum pump power of 3.10 W, maximum repetition rate of 81.96 kHz and shortest pulse duration of 1.37 μs were obtained. Meanwhile, maximum output power of 327.4 mW at a slope efficiency of 11.6% and single pulse energy of 3.99 μJ were also obtained and only limited by the available pump power. Note that this is also the most powerful and energetic passively *Q*-switched fiber laser using TI as the SA. These results suggest that TI is absolutely a class of high-performance broadband SA. Moreover, further increasing the repetition rate and decreasing the pulse duration are also possible by making a compromised optimization on the modulation depth of the TI: Bi_2Te_3 SA and the cavity length. In our experiment, the mode-locking was not observed. It can be explained by the CW mode locking condition:

$$E_p^2 > E_{\mathrm{sat},g} E_{\mathrm{sat},a} \Delta R, \tag{2}$$

where E_p is the intra-cavity pulse energy, $E_{\mathrm{sat},g}$ and $E_{\mathrm{sat},a}$ are the saturable energy of the gain medium and SA, respectively, and ΔR is the modulation depth of the SA. In this case, the small intra-cavity pulse energy caused by large unsaturable loss of the TI and small reflectivity of the output coupler, and large modulation depth of the TI make the above condition difficult to be satisfied. Therefore, the high-reflection output coupler and TI with comparatively low modulation depth and unsaturable loss are suggested to achieve mode locking. Moreover, the investigations on TI-based pulsed fiber lasers at longer mid-infrared wavelengths are also planned in the near future considering the long absorption wavelength edges of TI: Bi_2Te_3 (i.e., 8.28 μm) and its families, e.g., Bi_2Se_3 (i.e., 4.14 μm), Sb_2Te_3 (i.e., 4.44 μm), etc.

Funding. Open Found of Key Laboratory of High Energy Laser Science and Technology, CAEP (2013005580); Fundamental Research Funds for the Central Universities (ZYGX2013J058); National Natural Science Foundation of China (NSFC) (61377042, 61378028, 61435003); Open Fund of Medical Optical Key Laboratory of Jiangsu Province (JKLMO201403); Open Fund of State Key Laboratory of Advanced Optical Communication Systems and Networks (2015GZKF004); Program for New Century Excellent Talents in University of Ministry of Education of China (NCET-13-0094).

REFERENCES

1. J. Geng and S. Jiang, Opt. Photon. News **25**(7), 34 (2014).
2. R. Kaufmann, A. Hartmann, and R. Hibst, J. Dermatol. Surg. Oncol. **20**, 112 (1994).
3. H. H. P. T. Bekman, J. C. van den Heuvel, F. J. M. van Putten, and R. Schleijpen, Proc. SPIE **5615**, 27 (2004).
4. C. R. Petersen, U. Møller, I. Kubat, B. Zhou, S. Dupont, J. Ramsay, T. Benson, S. Sujecki, N. Abdel-Moneim, Z. Tang, D. Furniss, A. Seddon, and O. Bang, Nat. Photonics **8**, 830 (2014).
5. S. Tokita, M. Murakami, S. Shimizu, M. Hashida, and S. Sakabe, Opt. Lett. **34**, 3062 (2009).
6. P. Wan, L. Yang, S. Bai, and J. Liu, Opt. Express **23**, 9527 (2015).
7. O. Henderson-Sapir, J. Munch, and D. J. Ottaway, Opt. Lett. **39**, 493 (2014).
8. M. Bernier, V. Fortin, M. El-Amraoui, Y. Messaddeq, and R. Vallée, Opt. Lett. **39**, 2052 (2014).
9. J. F. Li, H. Y. Luo, Y. L. He, Y. Liu, L. Zhang, K. M. Zhou, A. G. Rozhin, and S. K. Turistyn, Laser Phys. Lett. **11**, 065102 (2014).
10. J. F. Li, D. D. Hudson, Y. Liu, and S. D. Jackson, Opt. Lett. **37**, 3747 (2012).
11. T. Hu, D. D. Hudson, and S. D. Jackson, Opt. Lett. **39**, 2133 (2014).
12. A. Haboucha, V. Fortin, M. Bernier, J. Genest, Y. Messaddeq, and R. Vallée, Opt. Lett. **39**, 3294 (2014).
13. C. Wei, X. S. Zhu, R. A. Norwood, and N. Peyghambarian, Opt. Lett. **37**, 3849 (2012).
14. C. Wei, X. S. Zhu, R. A. Norwood, and N. Peyghambarian, IEEE Photon. Technol. Lett. **24**, 1741 (2012).
15. C. Wei, X. S. Zhu, F. Wang, Y. Xu, K. Balakrishnan, F. Song, R. A. Norwood, and N. Peyghambarian, Opt. Lett. **38**, 3233 (2013).
16. M. Z. Hasan and C. L. Kane, Rev. Mod. Phys. **82**, 3045 (2010).
17. S. Q. Chen, C. J. Zhao, Y. Li, H. H. Huang, S. B. Lu, H. Zhang, and S. C. Wen, Opt. Mater. Express **4**, 587 (2014).
18. C. J. Zhao, H. Zhang, X. Qi, Y. Chen, Z. T. Wang, S. C. Wen, and D. Y. Tang, Appl. Phys. Lett. **101**, 21106 (2012).
19. G. Sobon, Photon. Res. **3**, A56 (2015).
20. J. Boguslawski, J. Sotor, G. Sobon, J. Tarka, J. Jagiello, W. Macherzynski, L. Lipinska, and K. M. Abramski, Laser Phys. **24**, 105111 (2014).
21. Z. H. Yu, Y. R. Song, J. R. Tian, Z. Y. Dou, H. Y. Guoyu, K. X. Li, H. W. Li, and X. P. Zhang, Opt. Express **22**, 11509 (2014).
22. Y. Chen, C. J. Zhao, S. Q. Chen, J. Du, P. H. Tang, G. B. Jiang, H. Zhang, S. C. Wen, and D. Y. Tang, IEEE J. Sel. Top. Quantum Electron. **20**, 0900508 (2014).
23. Y. Chen, C. J. Zhao, H. H. Huang, S. Q. Chen, P. H. Tang, Z. T. Wang, S. B. Lu, H. Zhang, S. C. Wen, and D. Y. Tang, J. Lightwave Technol. **31**, 2857 (2013).
24. L. Ren, X. Qi, Y. D. Liu, G. L. Hao, Z. Y. Huang, X. H. Zou, L. W. Yang, J. Li, and J. X. Zhong, J. Mater. Chem. **22**, 4921 (2012).
25. Q. K. Wang, Y. Chen, L. L. Miao, G. B. Jiang, S. Q. Chen, J. Liu, X. Q. Fu, C. J. Zhao, and H. Zhang, Opt. Express **23**, 7681 (2015).